arXiv:astro-ph/9805219v1 16 May 1998

Near Infrared Observations of a Redshift 4.92 Galaxy: Evidence for Significant Dust Absorption [1]

B.T. Soifer[2], G. Neugebauer[2], M. Franx[3], K. Matthews[2], G.D. Illingworth[4]

Received 1997 December 12; accepted 1998 May 15

[1]Based on observations obtained at the W.M. Keck Observatory

[2]Palomar Observatory, 320-47, Caltech, Pasadena, CA 91125

[3]Kapteyn Institute, P.O. Box 800, NL-9700 AV, Groningen, The Netherlands

[4]University of California Observatories / Lick Observatory, Board of Studies in Astonomy and Astrophysics, University of California, Santa Cruz, CA 95064

ABSTRACT

Near-infrared imaging and spectroscopy have been obtained of the gravitationally lensed galaxy at $z = 4.92$ discovered in HST images by Franx et al. (1997). Images at 1.2, 1.6 and 2.2μm show the same arc morphology as the HST images. The spectrum with resolution $\lambda/\Delta\lambda \sim 70$ shows no emission lines with equivalent width stronger than 100Å in the rest frame wavelength range 0.34μm to 0.40μm. In particular, [OII]3727Å and [NeIII]3869Å are not seen. The energy distribution is quite blue, as expected for a young stellar population with the observed Ly α flux. The spectral energy distribution can be fit satisfactorily for such a young stellar population when absorption by dust is included. The models imply a reddening 0.1 mag $< E(B-V) <$0.4 mag. The stellar mass of the lensed galaxy lies in the range of 2 to 16 $\times 10^9$ $M_\odot$. This is significantly higher than estimates based on the *HST* data alone. Our data imply that absorption by dust is important to redshifts of ~ 5.

Subject headings: Galaxies: formation; starburst

1. Introduction

The study of galaxies at high redshifts has been revolutionized with the introduction of the Hubble Space Telescope and the new generation of large ground-based telescopes. Detecting and studying such systems at high redshift is essential to understanding how normal galaxies form and evolve. Franx et al. (1997) have recently reported the serendipitous discovery of a field galaxy at a redshift $z = 4.92$ that has been gravitationally lensed into several arc components, including a highly magnified fold arc, by an intervening cluster of galaxies (CL1358+62) at $z = 0.33$. Franx et al. present HST imaging and Keck spectroscopy of this highly-magnified lensed system. Because of the redshift, the HST images at R ($F606W$) and I ($F814W$) correspond to wavelengths of 1023Å and 1375Å in the rest frame of the background objects, and thereby sample only the far UV portion of the light emitted from these galaxies. In order to study these objects at wavelengths where nearby galaxies have been studied, we observed the brightest (fold) arc of the lensed galaxy at near infrared wavelengths using the W.M. Keck Telescope. In the discussion we adopt the same cosmological parameters as in Franx, et al., i.e. $H_0 = 50$ Km/s/Mpc and q_0 =0.5.

2. Observations and Data Reduction

The observations reported here were made in April 1997 in photometric conditions using the near infrared camera (NIRC) at the f/25 forward Cassegrain focus of the W.M. Keck Telescope. The instrument is described in detail by Matthews and Soifer (1994). It has a 256×256 InSb array with $0.15'' \times 0.15''$ pixels for a $38'' \times 38''$ field of view.

Sets of images centered on the brightest portion of the arc (locations B to C, described by Franx et al. 1997) were obtained at 1.25μm (J), 1.65μm (H) and 2.2μm (K). The broadband J, H and K images were made with total exposures of 1620 s per filter. In

addition a set of images was taken in a 1.2% bandpass filter centered at a wavelength of 2.297 μm (rest wavelength 3881Å), which contained the redshifted [NeIII] 3869Å line). The total exposure time at this wavelength was 2700 s. The imaging data were obtained in sets of 60 s exposures, where the center of the field was moved in a 3×3 grid pattern 10″ on a side. The centers of successive grids were moved by 1–2″ between each set. Bright cluster galaxies in the frames were used to accurately register the successive frames for coaddition.

Sky and normalized flat-field frames were created from the data at each wavelength separately, taking the clipped mean of nine frames centered in time on the frame of interest. The seeing, as determined from several stellar images in the field, was approximately 0.5″ – 0.6″ FWHM. The data were calibrated using calibration stars of Persson (1997).

In addition to the images, low resolution grism spectra were obtained of selected sources within the arc. These spectra were obtained over the wavelength range 1.5 – 2.4μm (0.25 – 0.40 μm in the rest frame). The slit was 0.7″ wide yielding a spectral resolution of $\lambda/\Delta\lambda \sim 70$. Slit position angles of 80° and 145° were used. The brightest portion of the fold arc C, the knot and the northwest end (Franx et al. 1997) was contained in the slit for the PA 80° spectrum, while the slit was aligned with the arc for the PA 145° spectrum. For each position angle the integration time was 3000 s. The knot at the NW end of arc C was chosen because it was the brightest of the lensed knots, although the data of Franx et al show that the strength of Lyα is clearly lower at that position (the equivalent width of Lyα at this location drops to 1/3 of its value elsewhere in the arc).

3. Results

The J image of the field of CL1358+62 is shown in Figure 1a. Locations B and C in the nomenclature of Franx et al. (1997) are labeled. The arc is seen in the J, H and K images

over the entire spatial range in which it is visible in the HST images. The arc was also detected in the narrowband image at a level consistent with the K band continuum image and shows that the [NeIII] line does not contribute significantly to the flux (equivalent width <50 Å) in the arc.

In order to directly compare the Keck images with the HST image we have convolved the HST I image with the measured seeing of the Keck data. In Table 1 we report photometry at I, J, H and K in three beams; position 1 is a circular beam including the brightest peak in the arc at position C, position 2 includes the full arc from B to C with the beam shaped to mimic the arc but excluding the brightest knot, and position 3 is the sum of the first two beams. Figure 1b shows the shape of the beam of position 3.

To derive photometry that is less sensitive to the presence of the bright elliptical galaxy north-northeast of the fold arc, we first determined the surface brightness profile of this galaxy in each of the images using an ellipse fitting program. We subtracted the resulting model distribution from the images. This produced a flat background at the location of the arc that reduced the uncertainties in the photometry. The J band image formed in this way is shown in Figure 1b. To minimize the uncertainties in the photometry, we made the sky beam as large as possible while avoiding the field objects near the arc. The photometry obtained with and without the elliptical galaxy removed from the image was indistinguishable at all wavelengths. Because we felt the results were more robust, the photometry with the elliptical galaxy removed is reported in Table 1.

The spectrum at PA 80°, taken with the bright knot of the fold arc C centered in the slit, shows that the continuum was detected at low signal-to-noise ratio. No convincing detection of the arc was made in the spectrum at PA 145°. No lines were detected in either spectrum over the wavelength range 0.25 – 0.40 μm in the rest frame of the object. This corresponds to an upper limit on the equivalent width of 100 Å for any emission line

over the wavelength range 0.34 – 0.40 μm and a limit of 200 Å in the equivalent width of any emission line over the wavelength range 0.25–0.34μm (the higher limit at shorter wavelengths is a result of the strong OH airglow emission in the H band).

Since there is at best only marginal evidence for any color difference between positions 1 and 2, we adopt the highest signal-to-noise measurements of the sum of these apertures (position 3) to determine the intrinsic energy distribution of the source galaxy. This was determined by measuring the colors $I - [\lambda]$ at position 3 and subtracting these colors from the intrinsic $I_{AB,814} = 24.0$ mag of the lensed galaxy G1 determined by Franx et al. (1997). This leads to intrinsic (unmagnified) magnitudes for G1 of 22.4, 22.3, and 21.5 mag at J, H and K respectively. We do not believe that the quality of the data warrant interpreting the results in terms of color variations across the lensed object. In the discussion that follows the derived quantities refer to the intrinsic (unlensed) galaxy.

4. Stellar Population Models

The near infrared wavelengths correspond to rest frame UV and blue in the lensed galaxy, with the J, H, and K images being at 2150, 2790, and 3720 Å, respectively. The broadband colors potentially suffer from contamination by strong emission lines. In the K band the strongest potential contamination is due to [OII]3727Å emission. The limit of 100Å on the rest frame equivalent width of the [OII] line in the spectrum of the bright knot of C limits the contamination of the K continuum to <20% of the total observed flux in the band. This limit is consistent with that seen in young star–forming galaxies at $z \sim 1$ by Cowie et al. (1995), who find an average rest–frame equivalent width in [OII] of 60Å. The limit on [OII] equivalent width limits the increase in the spectral index due to line contamination in K to $\Delta\beta < 0.3$, where the spectral index is defined as $F_\lambda \propto \lambda^\beta$. In the H band, the strongest potential contaminant is MgII 2800Å, while in the J band

it is CIII] 1909Å. Our limit on the MgII line is not particularly significant, while we do not have spectra covering the CIII] wavelength. The CIII] and MgII lines are not seen in the nuclear spectra of nearby starbursts such as NGC 4214 (Leitherer et al. 1996) or blue compact galaxies such as Haro 2 (Thuan 1990), while our limit on [OII]3727Å is consistent with the strongest lines seen in nearby blue galaxies by Gallagher et al. (1989). Thus we conclude that the effect of line emission on the derived colors is at most comparable to the uncertainties in the observations.

The slope of the continuum is well characterized by $F_\lambda \propto \lambda^{-1.63}$. Although this is fairly blue, it not as blue as models predict for young, ionizing starburst populations (e.g., Leitherer and Heckman 1995). Most of their models predict a slope < -2.2 for ages smaller than 10^7 years (as needed for the observed Ly α – see below). The redder colors we observe can be produced either by dust, or by the presence of older stars. In both cases the mass of the stellar population would be seriously underestimated if the masses are estimated from the bluest passband. To address this issue, we made fits to the spectral energy distribution using the models by Bruzual and Charlot (1993, 1996). We considered models for populations with instantaneous starbursts and with constant star formation rates and have included the effect of reddening.

The results are shown in Figure 2. Instantaneous starburst models with ages between 3×10^5 and 10^7 years are shown in Figures 2a and 2c. The age of the burst population has to be lower than 10^7 years to provide the ionizing flux for the Ly α emission. The IMF was assumed to be a Salpeter law. Figure 2a shows models with no reddening fit to the data including the I photometry, while figure 2c shows models fit to the data where reddening is a free parameter. The models can provide good fits with a dust reddening $E(B-V)$ between 0.26 and 0.37 mag, but do not fit the data satisfactorily when reddening is not included. The masses of the stellar population were in the range of 5 to 16×10^9 $M_\odot$.

Models with continuous star formation can also provide a good fit to the data once reddening is considered. Figures 2b and 2d show models with ages up to 10^9 years. We do not consider models with ages $> 10^9$ years since this is approximately the Hubble time at z=4.92. As with the instantaneous burst models, the models in figure 2b assume no reddening, while in figure 2d reddening is a free parameter in the fit, and these models provide signficantly better fits than the dust free models. The required reddening $E(B-V)$ lies between 0.15 and 0.39 mag. The required star formation rates lie between 130 and 4×10^4 $M_\odot yr^{-1}$. The total stellar masses range from 7 to 30×10^9 $M_\odot$, for ages from 10^7 to 10^8 years, respectively. The mass becomes progressively larger with even greater ages. As can be seen in Figure 2d, the models with ages $\geq 10^8$ years predict a strong Balmer break, and this significantly reduces the quality of the fit. At an age of 10^9 yr, the total chi square for the dust free model is 40, while that containing dust is 4.6. The observed equivalent width of Ly α between 7 and 21 Å does not provide a strong constraint on these continuous star forming models.

The new data result in much higher mass estimates than the earlier estimates (Franx et al. 1997) which were derived from the rest-frame far-UV flux (observed HST I_{814}). The masses are increased because the fluxes in the new redder passbands are significantly higher than predicted by the (dust free) models used by Franx et al. An additional dependency with these new mass estimates is on the form of the extinction curve used. The Calzetti et al. (1994) extinction curve is rather grey. If we use an SMC extinction curve, we find that the absorption and stellar masses are decreased by a factor of about two.

We can also estimate masses by ignoring the extinction and simply using the reddest flux, i.e., the observed K band flux, or restframe U. We obtain masses of 1.1 to 5×10^9 $M_\odot$ for the instantaneous burst models, and masses between 1.6 and 9×10^9 for the continuous star formation models. These estimates are roughly one quarter of the estimates derived by

using the Calzetti et al. (1994) extinction curve, and about half the estimate derived from the SMC extinction curve. We conclude therefore that the uncertainty in the mass estimate is about a factor of four.

A realistic assessment of the likely mass is given by the geometric mean of the no-reddening values and the values based on the Calzetti et al. (1994) extinction curve: masses between 2×10^9 and 9×10^9 $M_\odot$ for instantaneous bursts, and between 3×10^9 and 16×10^9 $M_\odot$ for continuous star formation models.

5. Discussion

The discussion of the last section has shown that the lensed galaxy has significant extinction, and we have derived new larger estimates for the stellar mass. The high stellar masses imply that the galaxy has built up a very dense center. The knot, which has an effective radius of 130 pc, contains roughly half the mass, i.e., 1.2 to 8×10^9 $M_\odot$ (Franx, et al, 1997). Assuming an isothermal profile, we derive a velocity dispersion of the knot between 100 and 260 km s^{-1}. Our new results have therefore strengthened the case that this young galaxy at $z = 4.92$ has already managed to build up a very dense core.

The resulting dynamical timescale for the knot is a few times 10^6 year, comparable to the age derived from a starburst model. The dynamical timescale for the galaxy as a whole is at least 10 times higher. This exceeds the lifetime of ionizing O stars. Combined with the fact that the emission and absorption line properties observed by Franx et al. (1997) indicate the presence of a strong wind which locally depletes the interstellar medium in this galaxy, it is likely that we are seeing young, short lived condensations of star formation. Over time, these knots would brighten progressively across the galaxy, as suggested earlier by Lowenthal et al (1997).

The infrared photometry has demonstrated that dust is very likely present in the galaxy. This conclusion clearly depends on the accuracy of the stellar evolutionary models. The reddening is estimated to be between 0.1 mag$< E(B-V) < 0.4$ mag, depending on the population model and extinction curve. These values are comparable to those found in nearby, low metallicity, starbursts (e.g., Meurer et al 1997. This implies that the galaxy has been able to produce a significant amount of metals, but the observations to date are inadequate to derive metallicities.

We note that similar results were derived by Ellingson et al. (1996) for MS1512-cB58 and for galaxies in the Hubble Deep Field by Sawicki and Yee (1998). The optical and infrared fluxes of MS1512-cB58 at $z = 2.72$ imply a young age (10^7 years) and a significant extinction ($E(B-V) \sim 0.3$ mag). The constraints on the age of the young population were stronger because the observations extended beyond the Balmer break. In the case of the Hubble Deep Field, Sawicki and Yee have found that spectral energy distributions with reddening of $E(B-V) \sim 0.3$mag provides better fits to the observations of $z > 2$ Lyman Break galaxies than do dust free models. The best studied high redshift galaxies have significant amounts of dust while evidence for dust exists for other high redshift galaxies based on sparser color information (e.g., Meurer et al. 1997, Pettini et al. 1997). If the lensed galaxies are typical, then a reddening between $E(B-V) \approx 0.2 - 0.3$ mag should be expected for most high redshift galaxies.

We thank W. Harrison for assistance with the observations, and S.E. Persson for providing photometric standards in advance of publication. The W.M. Keck Observatory is operated as a scientific partnership between the California Institute of Technology, the University of California and the National Aeronautics and Space Administration. It was made possible by the generous financial support of the W.M. Keck Foundation. Infrared astronomy at Caltech is supported by grants from the NSF and NASA. Support from STScI

grant GO05989.01-94A is also gratefully acknowledged. This research has made use of the NASA/IPAC Extragalactic Database which is operated by the Jet Propulsion Laboratory, Caltech, under contract with NASA.

Table 1: Photometry of Locations in lensed arc in CL1358+62

Position	Beam	I[a]	J	H	K
		mag	mag	mag	mag
1	circ [b]	22.88±0.04	21.7 ±0.2	21.6±0.3	21.3 ±0.3
2	arc [c]	22.79±0.04	21.84±0.20	21.40±0.30	20.54 ±0.18
3	irr [d]	22.11 ±0.03	20.92 ±0.11	20.83 ±0.22	19.99±0.14

[a]The magnitude referred to here as I is that from the HST image in the F814W filter from the data of Franx, et al. 1997.

[b]Photometry refers to a 1.8″ diameter circular beam, centered on object C (in nomenclature of Franx et al.)

[c]Photometry refers to arc shaped beam that includes object B and the arc between B and C (in nomenclature of Franx et al.)

[d]Photometry refers to an irregular shaped beam that includes both objects B and C and the arc between them (the sum of positions 1 and 2)

REFERENCES

Bruzual, G. and Charlot, S. 1993, ApJ, 405, 538

Bruzual, G. and Charlot, S. 1996, in preparation

Calzetti, D., Kinney, A.L. and Storchi-Bergmann, T. 1994, ApJ, 429, 582

Cowie, L.L., Hu, E.M. and Songaila, A. 1995, Nature, 377, 603

Ellingson, E., Yee, H. K. C., Bechtold, J., 1996, ApJ, 466, L71

Franx, M., Illingworth, G.D., Kelson, D.D., van Dokkum, P.G. and Tran, K-V. 1997, ApJ, 486, L75

Gallagher, J.S., Bushouse, H. and Hunter, D.A. 1989, AJ, 97, 700

Leitherer, C. and Heckman, T.M. 1995, ApJS, 95, 9

Leitherer, C., Vacca, W.D., Conti, P.S., Filippenko, A.V., Robert, C. and Sargent, W.L.W. 1996, ApJ, 465, 717

Lowenthal, J. D., Koo, D. C., Guzman, R., Gallego, J., Phillips, A. C., Faber, S. M., Vogt, N. P., Illingworth, G. D., & Gronwall, C., 1997, ApJ, 481, 673

Matthews, K. and Soifer, B.T. 1994, *Infrared Astronomy with Arrays: the Next Generation, I. McLean ed.* (Dordrecht: Kluwer Academic Publishers), p.239

Meurer, G.R., Heckman, T.M., Lehnert, M.D., Leitherer, C. and Lowenthal, J. 1997, AJ, 114,54

Persson, S.E. 1997, in preparation

Pettini, M., Steidel, C.S., Adelberger, K.L., Kellogg, M., Dickinson, M. and Giavalisco, M, 1997, astro-ph 9708117

Sawicki, M. and Yee, H.K.C. 1998, AJ, 115, 1329

Scoville, N.Z and Young, J.S. 1983, ApJ, 265, 148

Thuan, T.X. 1990, *Massive Stars in Starbursts, C. Leitherer, N. Walborne, T. Heckman and C. Norman, eds* (Cambridge: Cambridge University Press), p183

Fig. 1.— Image of Lens Arc associated with the cluster CL1358+62 in the J band obtained with the W.M.Keck Telescope. The top panel is the image of the field with the orientation indicated in the image, the bottom panel is the same image with the lensing galaxy removed. Locations B and C from Franx, et al. are indicated in the top image, while the outline of the photometric aperture C is shown in the bottom image.

Fig. 2.— The energy distribution for the lensed system in CL1358+62, plotted as luminosity density vs. rest wavelength compared with instantaneous and continuous star formation models from Burzual and Charlot (1993, 1996). The left panels, represent instantaneous models of ages 10, 30 and 100 $\times 10^5$ years, the top panel being unreddened, the bottom panel having a reddening E(B-V) between 0.23 and 0.33 mag. The right panels represent continuous star formation models with ages of 3, 10, 30, 100, 300, 1000 and $10,000 \times 10^5$ years. The top panel is unreddened models, the bottom panel having reddening between 0.15 and 0.39 mag to best fit the data, with the older models requiring less reddening. For both sets of models, ages below the youngest listed age are indistinguishable.

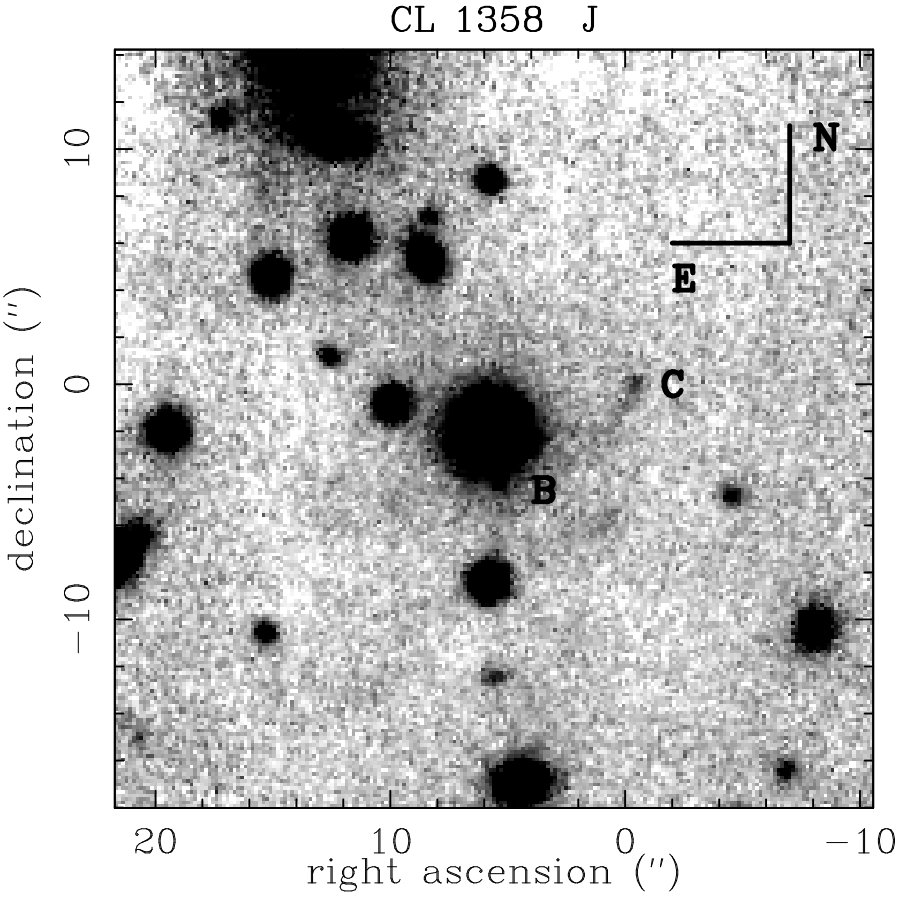
CL 1358 J
N
E
C
B
declination (″)
10
0
−10
20
10
0
−10
right ascension (″)

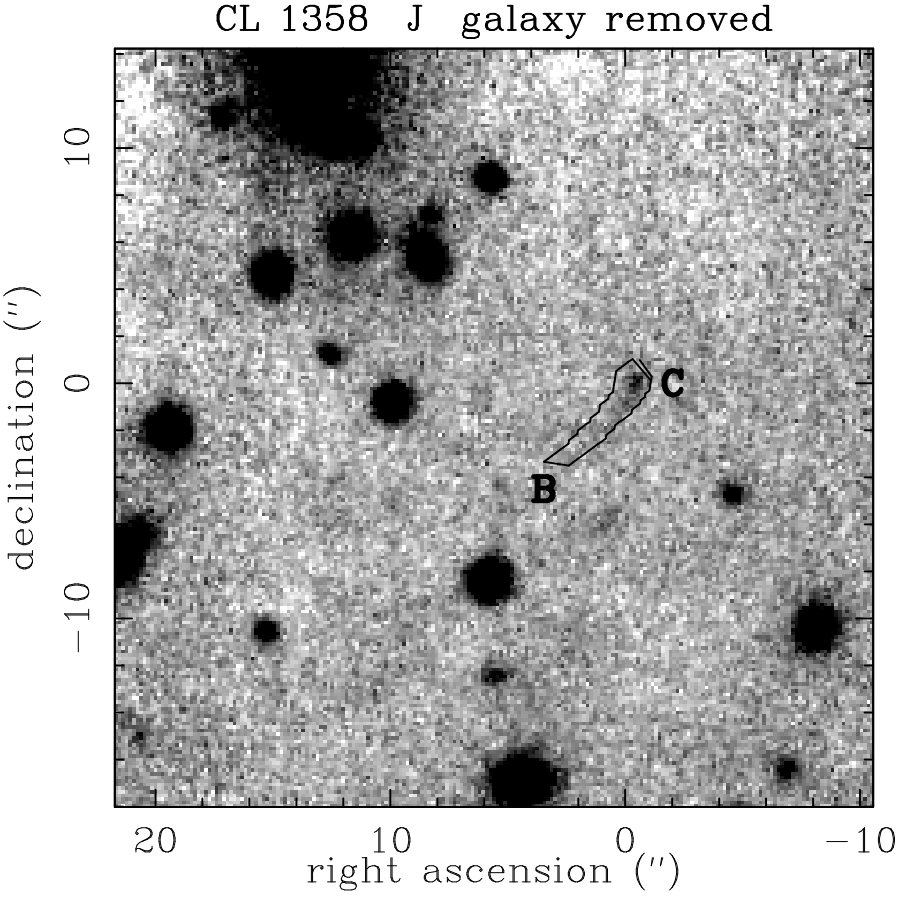
CL 1358 J galaxy removed
C
B
declination (″)
10
0
−10
20
10
0
−10
right ascension (″)

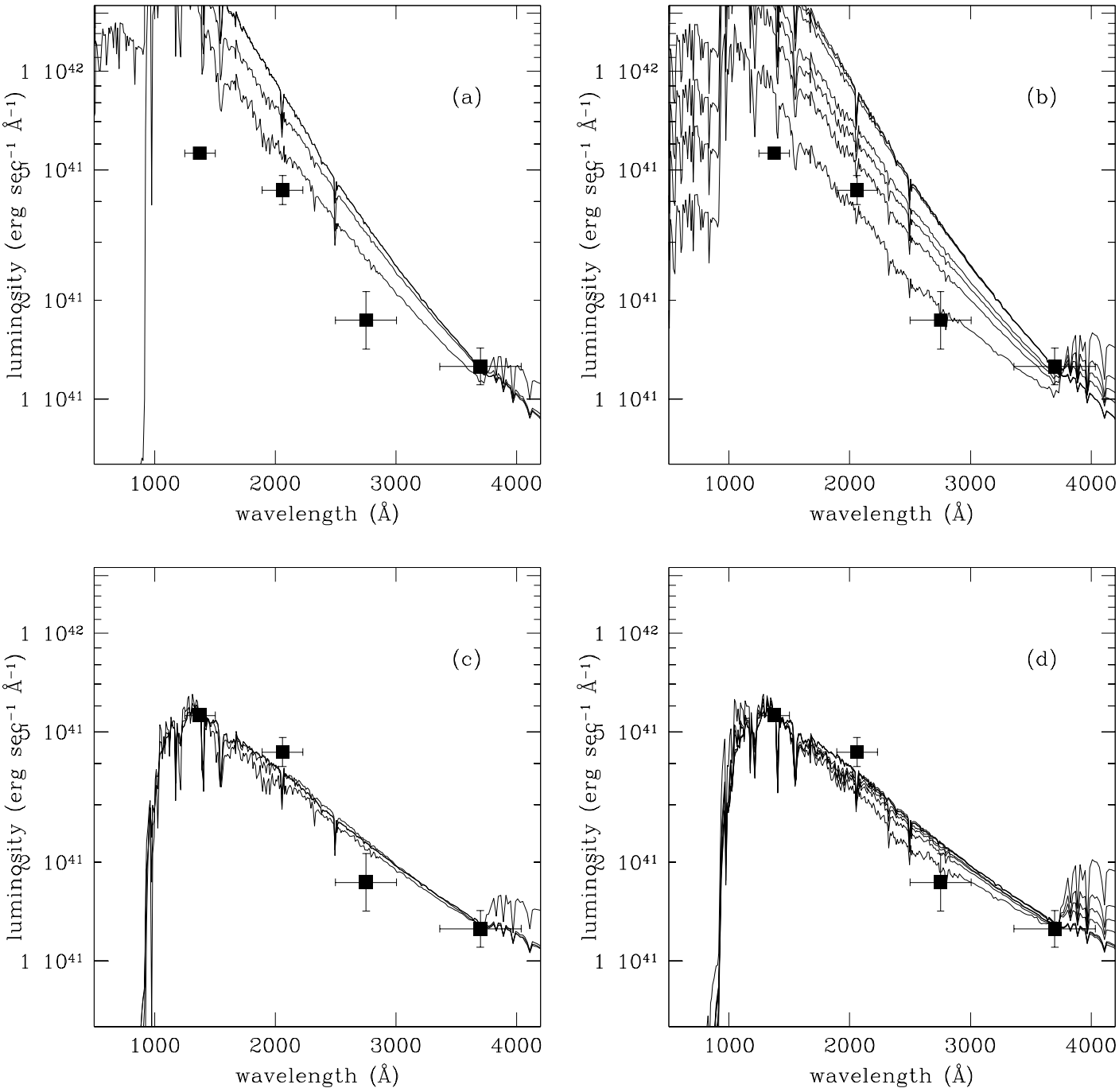
(a)
(b)
(c)
(d)
luminosity (erg sec^{-1} Å^{-1})
wavelength (Å)
1 10^{42}
1 10^{41}
1000
2000
3000
4000